Journal of Cement Based Composites 4 (2022) 5736
Cement Based Composites
journal home: www.acapublishing.com/journals/5/cebacom

Research Article

Hysteretic Performance of Hybrid GFRP-Steel Reinforced Concrete Shear Walls: An Experimental Investigation

Hany el-Kady[1], Osama Amer*,[1], Ahmed H. Ali[2], Hesham Haggag[3]
[1]Department of Civil Engineering Helwan University, Cairo, Egypt
[2]Department of Civil Engineering, Ain Shams University, Cairo, Egypt

Keywords

Reinforced concrete, Seismic performance, Fundamental period, RC shear wall, glass fibre-reinforced polymer (GFRP) bars

Abstract

The vulnerability of steel reinforcement to corrosion is a severe problem affecting the overall performance and durability of concrete structures in aggressive environments. The interest in using alternative Glass fibre-reinforced polymer (GFRP) bars lies in their corrosion resistance and higher tensile strength-to-weight ratio. Nevertheless, experimental results on the seismic behaviour of GFRP-reinforced walls are scarce. This paper investigates the hysteretic performance of hybrid steel-GFRP reinforced concrete shear walls to provide valuable experimental evidence for such walls under seismic loading. Six RC shear walls with steel and GFRP reinforcement were tested under pseudo-static reversed-cyclic lateral load. Three shear walls were reinforced by GFRP bars as longitudinal and transversal reinforcement, and two walls were reinforced with hybrid GFRP-steel bars with different ratios of web reinforcement. A reference specimen, ordinary steel-RC shear walls, was also introduced to certify the capability of GFRP as reinforcement bars. The results indicated that the GFRP-reinforced concrete slender walls had a stable hysteretic response and slight residual drift up to failure. Lower residual deformations, higher displacement capacity, and increased lateral strength could be observed with the GFRP web reinforcement ratio increase. Moreover, the fundamental period of GFRP and hybrid GFRP-steel reinforced walls can reach more than twice its original value prior to failure.

1.Introduction

The fact that reinforced concrete shear walls offer high lateral strength, stiffness, and deformation capacity under seismic loading makes them a standard option for lateral load-resisting structures. Understanding the response and behaviour of shear walls is crucial for accurately assessing their failure mechanisms and producing more reliable and economical designs, especially now that performance-based design methods are more prevalent for new structures [1]. Previous studies [2] defined a shear strength failure criterion for shear walls. The study assembled and reviewed a database of existing tests on lightly reinforced shear walls. The results indicated the most important factors that affect the nominal shear strength, which included the presence of axial load, the amount of boundary reinforcement provided, and the location of weak plane joints on the wall.

Typically, shear walls resist small frequent seismic and wind loads through an elastic manner where deformations remain within the yielding limit. However, ductile deformations without a considerable loss in strength are required to withstand more significant and less frequent earthquakes. Seismic energy is dissipated by ductile behaviour, which also minimizes structure collapse. Desirable ductility for shear walls is reached when the failure mode is dominated by flexure. Additionally, other non-ductile failure modes, such as compression failures or diagonal tension (shear failures), anchorage slip failure, and sliding shear failure, should be prevented [3]. These failure modes occur due to inadequate shear capacity and insufficient stiffness of the walls. Among the other deficiencies leading to these undesirable modes of failure are the lack of anti-buckling and confinement reinforcement, as well as deficient lap splices and insufficient anchorage length [4,3].

As conventional steel has long been the most commonly used reinforcement for concrete structures, its vulnerability to corrosion poses a severe challenge for structures located in aggressive environments. Conversely, GFRP reinforcing bars are inherently immune to corrosion, which offers a desirable alternative to conventional steel reinforcement for reinforced concrete structures, including columns, beams, and one-way and two-way slabs [5-10].

According to Deitz et al. [11], the GFRP rebar's compressive Youngs modulus is approximately equivalent to its Youngs modulus in tension. Chen et al. [12] studied the tensile behaviour of embedded GFRP bars in concrete members to predict its long-term behaviour. At temperatures 20, 40, and 60°C, The GFRP bars were exposed to simulated concrete pore solutions (water, salt solution, and alkaline solutions of various concentrations). According to the test results, high temperatures increased moisture accessibility to the bar, and alkalinity of the moisture all accelerate the degradation of the tensile and bond strength of GFRP bars. An experimental investigation on GFRP-reinforced shear walls under lateral cyclic loading was conducted by Mohamed et al. [13]. The results revealed that properly designed GFRP-reinforced shear walls would attain their flexural strengths without significantly degrading. Higher deformation capacity can also be achieved for GFRP-reinforced squat walls if it was properly designed and detailed [14]. Moreover, according to Afifi et al. [15], using closely spaced GFRP transverse reinforcement with a small diameter can result in more effective confinement and ductility than to large diameter with more spacing. The impact of spiral transverse GFRP bars on the structural performance of shear walls was recently studied by Hosseini et al. [16]. The walls were tested under constant axial load and cyclic lateral loading. The result revealed that transverse spiral bars could improve the shear and displacement capacities of the walls. However, compared to the steel-reinforced walls, the GFRP bars reduced the displacement ductility and dissipated energy.

*Corresponding Author: osama_amer@cu.edu.eg
Received 20 Oct 2022; Revised 21 Oct 2022; Accepted 24 Oct 2022
https://doi.org/10.36937/cebacom.2022.5736

The present study is oriented to investigate the applicability of GFRP bars for reinforced concrete shear walls either as a primary reinforcing element or in a Hybrid GFRP-steel reinforcement. The study presented focuses on examining the behaviour and response of GFRP-RC shear walls, intending to improve the knowledge of its failure mechanisms under seismic loading.

2. Material And Methods

The experimental program comprised the testing of six full-scale reinforced concrete (RC) shear walls under quasistatic cyclic loading up to the failure. The tested walls included one reference steel-reinforced specimen (SW1), three GFRP-reinforced specimens (GW1, GW2, and GW3), and two walls with hybrid GFRP-steel reinforcement (SGW1 and SGW2) (Figures 1 and 2).

Normal-weight and ready-mixed Concrete with a targeted concrete compressive strength (f_c') of 30 MPa was used for the construction of all tested specimens. Water to cement ratio (w/c) of 0.4 was adopted for all walls where the water and cement contents were 160 kg/m^3 and 400 kg/m^3, respectively. The aggregate content was 1700 kg/m^3 with a maximum aggregate size of 10 mm.

Steel bars of Grade 240/350 were used for horizontal reinforcement, and Grade 400/600 steel bars were used for vertical reinforcement. Moreover, #4 sand-coated straight GFRP reinforcing bars were used for the horizontal and vertical reinforcement (Table 1). A displacement-controlled hydraulic actuator with a maximum capacity of $\pm 500kN$ (pushing/pulling) and a total stroke of $\pm 250mm$, which was anchored to a strong reaction frame, was used to impose the lateral cyclic loading in the push and pull directions.

Table 1 - Material properties of adopted reinforcements

Steel bars	$d_b(mm)$	$A_s(mm^2)$	$E_s(GPa)$	$f_y(MPa)$	$\varepsilon_y(\%)$
	8	50.3	200	400	0.2
	12	113			
GFRP bars #4	$d_b(mm)$	$A_f(mm^2)$	$E_f(GPa)$	$f_{fu}(MPa)$	$\varepsilon_{fu}(\%)$
	12.7	126.7	69.6	1392	2.0

d_b donates the diameter of reinforcing bar. A_s and A_f represent the area of steel and GFRP reinforcement bars, respectively. E_s and E_f are the modulus of elasticity of steel and GFRP reinforcement, respectively.
f_y and ε_y are the specified yield strength and strain for steel bars, respectively. f_{fu} and ε_{fu} the design tensile strength and rupture strain of GFRP bars.

Quasi-static cyclic lateral loading was applied using a displacement-controlled hydraulic actuator with a total stroke of ±250mm and a maximum capacity of ±500kN (pushing/pulling. The actuator was anchored to a strong reaction frame, as shown in Figure 3. The imposed lateral loading protocol (Figure 3b)comprised two fully-reversed lateral drift cycles. Different internal and external instrumentations were used to record critical response quantities (loads, strains, displacement, and rotation) in each wall specimen. Linear variable differential transformers (LVDTs) were used for measuring top lateral displacements, axial deformations, concrete strain, and base sliding.

3. Results and discussion

3.1. Backbone curves

The envelope curves of load-drift and moment-rotation response are presented and compared for all tested walls in Figure 4. The lateral load was normalized for each specimen to facilitate comparison between the walls, as shown in Figure 4b, where the peak lateral load was chosen as the datum point, and the envelope curves of each wall were normalized based on the datum point.

Prior to cracking, all walls exhibited almost the same initial curve slope. With additional loading, steel and hybrid steel-GFRP reinforced walls had higher effective stiffness due to the higher elastic modulus of steel bars than GFRP bars. The results also showed that the steel and hybrid steel-GFRP reinforced walls exhibited ductile behaviour characterized by lower stiffness degradation at earlier drift levels and a relatively small strength degradation with increasing displacement after reaching the ultimate load. Conversely, GFRP-RC walls had lower ductility compared to the steel-reinforced wall. Moreover, walls GW2 and GW3, which had a higher reinforcement ratio than wall GW1, experienced higher lateral load and displacement capacities but less ductility and more distinct stiffness degradation at earlier drift levels than GW1.

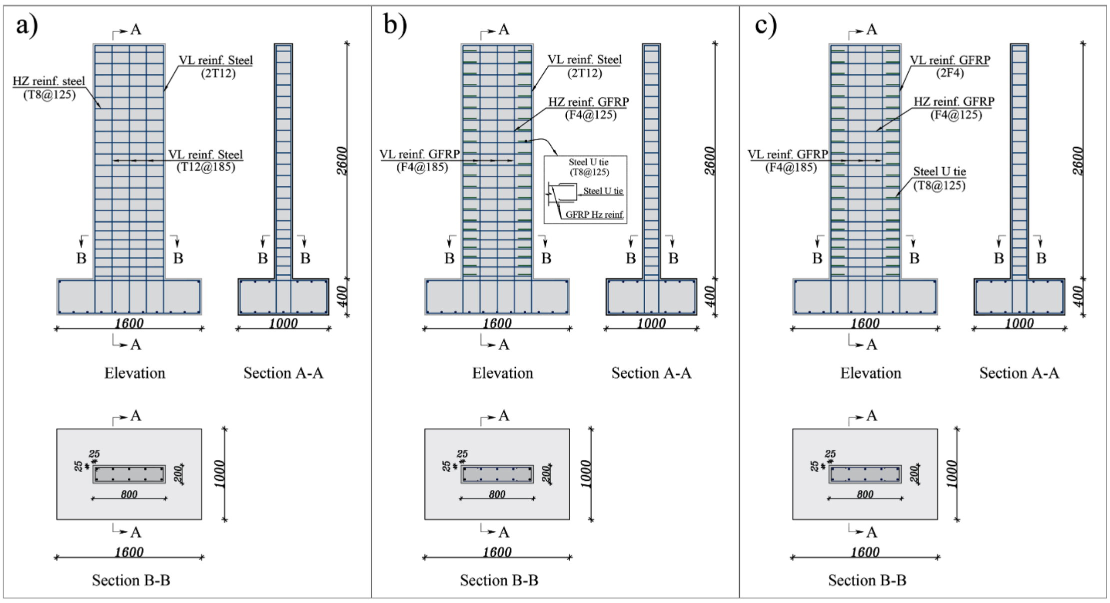

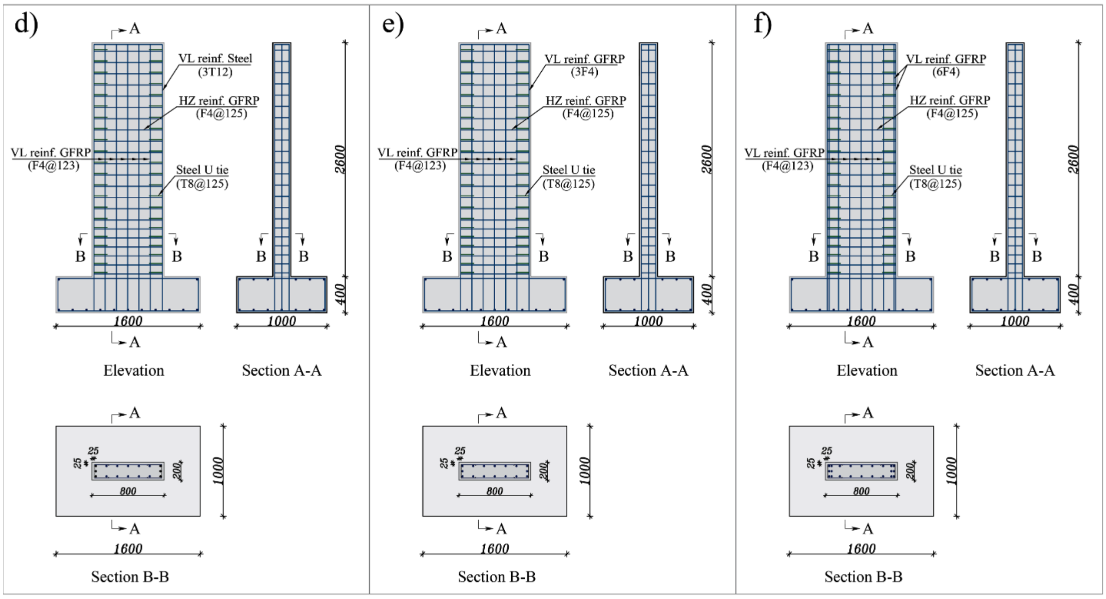

Figure 1 – Concrete dimensions and details of reinforcement configuration of walls (a) SW1 (b) SGW1, (c) GW1, (d) SGW2, (e) GW2, and (f) GW3. All dimensions in mm

3.2. Damage propagation and plastic hinge formation

For steel-reinforcement walls, at a higher displacement level, vertical splitting cracks of the concrete cover initiated at the compression end of the wall when the concrete compression strain ranged between 0.003 and 0.0035, corresponding to a drift of 1.44%, 1.55%, and 1.83% for walls SW1, SGW1, and SGW2, respectively. During consecutive cycles, spalling of the concrete cover became more significantly associated with longitudinal-bar buckling, and plastic hinges near the base were developed, as shown in Figure 5. Plastic deformations were kept developing in the formed plastic hinge zones until complete cover spalling occurred due to the exhibited high capacity for inelastic elongation of steel bars.

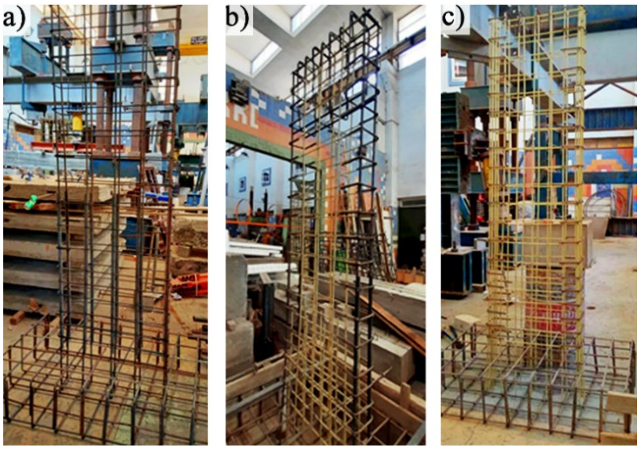

Figure 2 – Reinforcement configuration of (a) steel, (b) hybrid steel-GFRP, and (c) GFRP reinforced walls

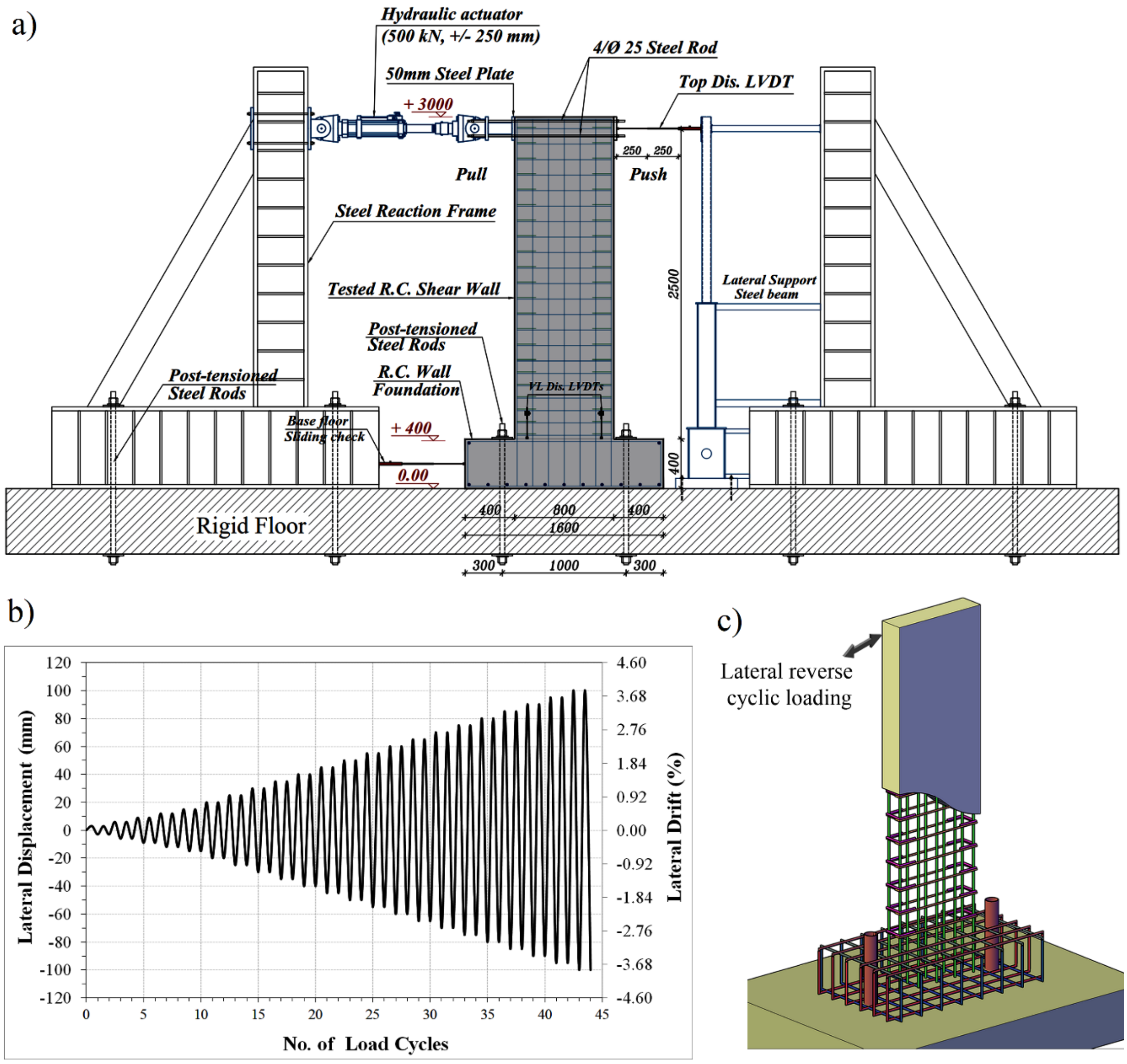

Figure 3 - Layout of the test setup and used LVDTs (a), Applied displacement-controlled loading history (b) and (c) schematic 3d view of the tested walls

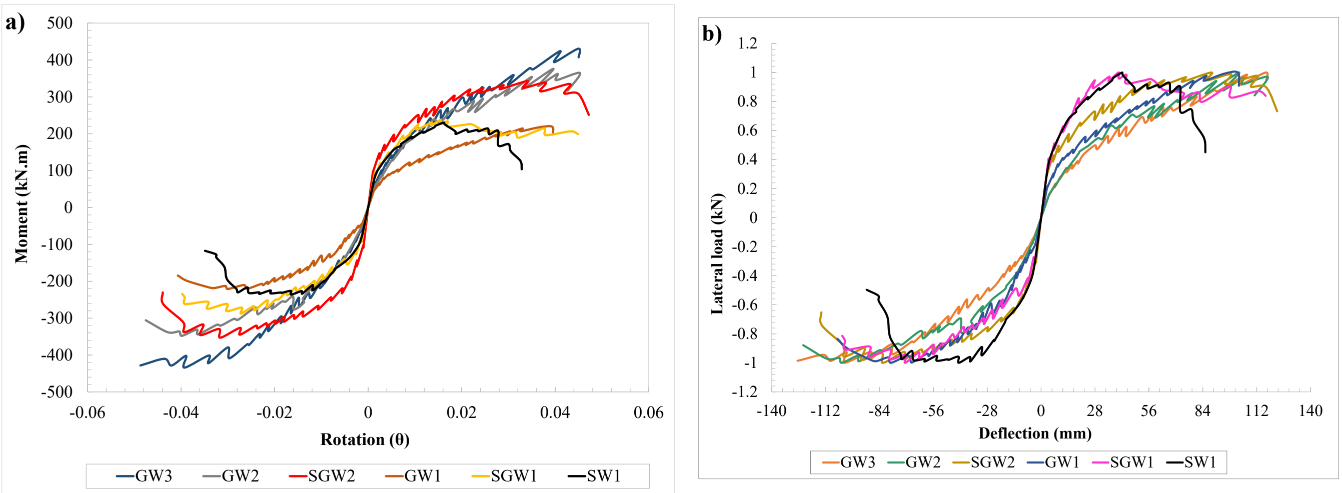

Figure 4 – Envelope curves of the test walls: a) moment-rotation envelope curves, and b) normalized load-displacement envelope curves

On the other hand, the developed plastic hinges in GFRP-reinforced walls were associated with the localized compression strain in the outmost heavily compressed end of the walls (Figure 6). The envelope of measured crack widths for all tested walls is illustrated in Figure 7. Visual measurements were conducted to determine the plastic hinge length developed during the experiments. The length of developed plastic hinges, l_p, was considered as the height where concrete splitting cracks and cover spalling exist. The plastic hinge height measured approximately 197, 270, and 242mm for steel-reinforced walls SW1, SGW1, and SGW2, which is 0.25, 0.33, and 0.3 of the wall length, l_w, respectively. It is noted that higher vertical reinforcement ratios forced the walls to initiate a more significant number of horizontal flexural cracks, diagonal shear cracks, and secondary flexural cracks. The developed secondary cracks redistribute the high tensile stresses in the outermost vertical reinforcing bars over a more considerable length, spreading the high curvatures at the base of the wall over a more extensive zone and extending the plastic hinge length.

For the GFRP-reinforced walls, higher heights were measured for the plastic hinges due to the highly elastic behaviour of GFRP bars and the increased localized compression strain at the concrete end of the walls. On the contrary, the effect of the primary cracks in steel-reinforced walls leads to the concentration of the steel plasticity at damaged locations, consequently localizing the plastic hinge length over a relatively small height above the foundation level. Approximate values of 210, 504, and 605mm were found for the plastic hinge developed in SW1, SGW1, and SGW2 walls corresponding to 0.26, 0.63, and 0.75 of the wall length, l_w, respectively.

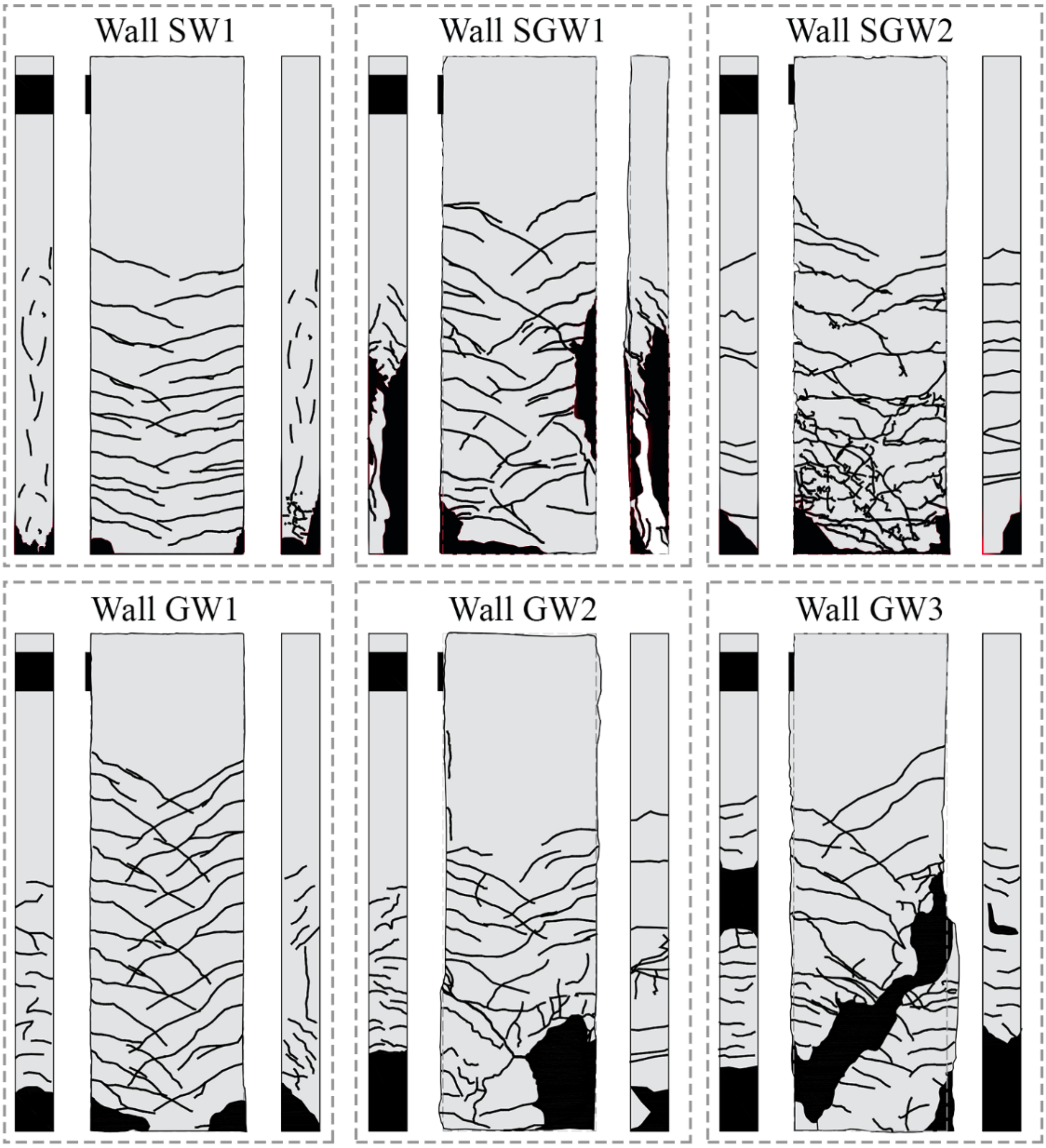

Figure 5 – Crack patterns for all tested walls

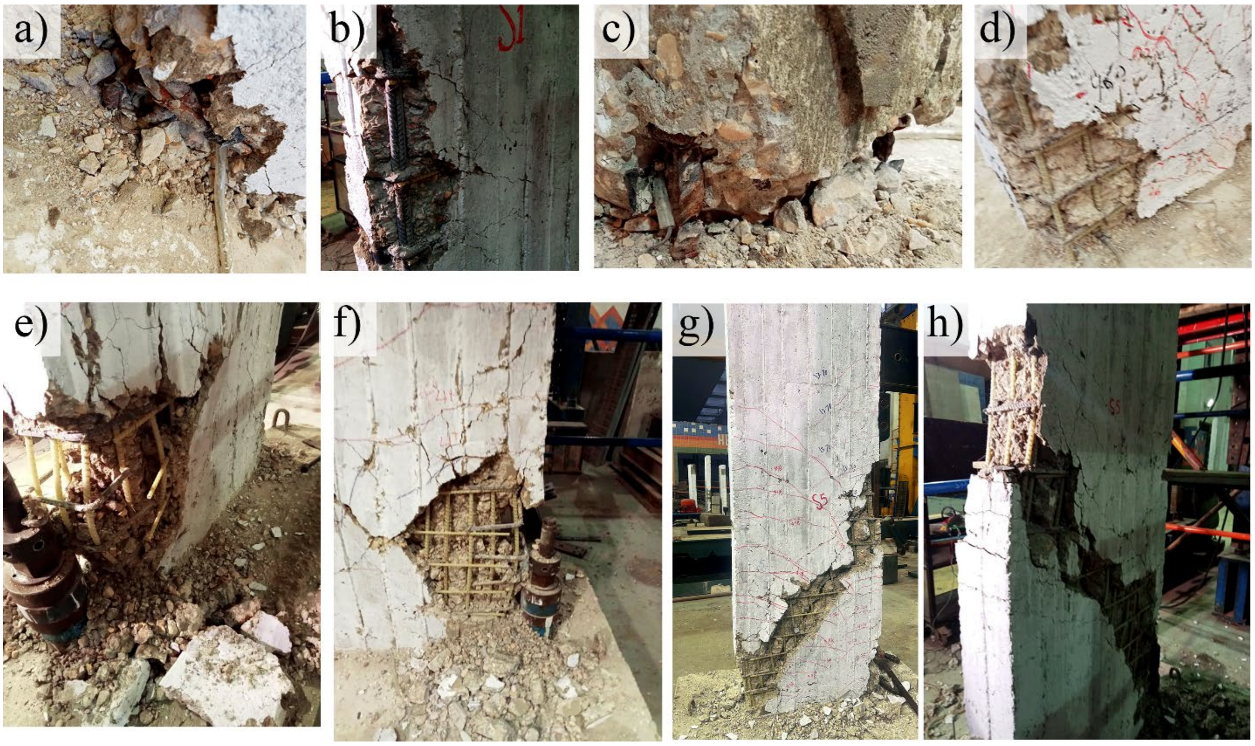

Figure 6 – Damage observed at failure of walls a) SW1, b) SGW1, c) SGW2, d) GW1, e-f) GW2, and g-h) GW3

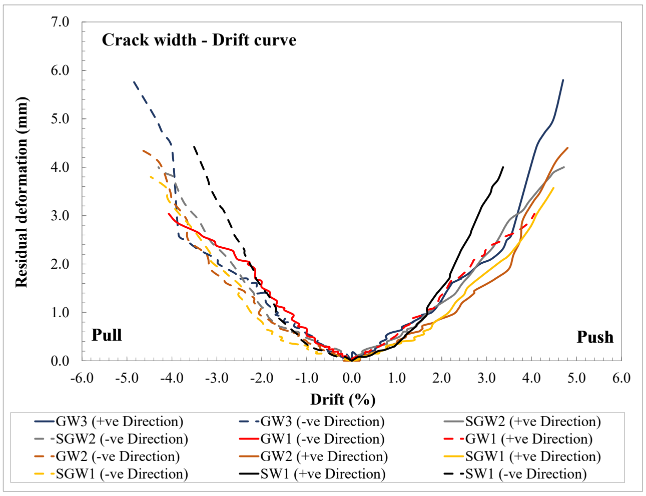

Figure 7 – Envelopes of measured crack width against drift

3.3. Hysteretic stiffness and fundamental period shift

The obtained hysteretic behaviour of the tested walls showed that the strength and stiffness of the specimens decreased in the inelastic stage, indicating the accumulated damage that the walls experienced under reversed lateral cyclic loading. Consequently, the effective secant stiffness ($K_{s,i}$) was calculated at each drift level and normalized to the initial stiffness (K_{init}) to investigate the stiffness degradation over the consecutive drift levels. The initial stiffness was calculated as secant for the first load step then the effective secant stiffness of each following loop was obtained as the slope of a straight line passing through the corner points of the loop. The normalized stiffness was then plotted versus the drift at different cycles in Figure 8. According to the obtained results, as higher deformations were induced, a similar pattern of stiffness degradation was seen for all the walls; however, higher degradation rates were attained in the GFRP-reinforced walls than those of steel-reinforced. Average reductions in K_{init} upon initial cracking of steel and hybrid steel-GFRP reinforced walls were 29.5%, 31%, and 36.3% for walls SW1, SGW2, and SGW3, respectively. On the other hand, for the GFRP-reinforced walls GW1, GW2, and GW3, respectively, the secant stiffness was rapidly decreased to, on average, 33.5%, 34.8%, and 34.9%.

At higher drift levels, further degradation remained at relatively low values of around 5%, 7%, and 13% of K_i for walls SW1, SGW1, and SGW2, respectively. However, lower stiffness degradation rates were attained for walls GW1, GW2, and GW3, reaching 9%, 14%, and 17%, respectively. Thus, the results obtained showed that, as higher deformations were imposed, the hybrid steel-GFRP reinforced walls exhibited a lower rate of stiffness degradation than GFRP-reinforced walls. Nevertheless, at higher drift levels, the higher stiffness degradation rate of steel and hybrid steel-GFRP reinforced walls was eventuated due to the occurred severe damage after yielding, which affected their ability to sustain the much-imposed load.

Furthermore, reliable evaluation of the magnitude and effects of the fundamental vibration period for lateral resisting RC structures constitutes an essential step in estimating earthquake-induced forces and assessing their seismic response. The fundamental period of RC structures mainly depends on their mass and effective stiffness; consequently, it depends on their dimensions, morphology, and irregularities, among other factors that may affect their effective stiffness [17]. The period value of RC structures appears in formulas specified in most design codes to compute the design base-shear and resultant lateral forces. An increase in the fundamental period due to concrete cracking will most likely reduce the earthquake-induced forces in the case of RC structures with a fundamental period higher than $0.5\ sec$. However, for RC structures with a fundamental period lower than $0.2\ sec$, an increase in the period may increase the earthquake forces [18]. Consequently, an accurate prediction of the fundamental period and its effect is significantly required for the seismic assessment of RC shear walls.

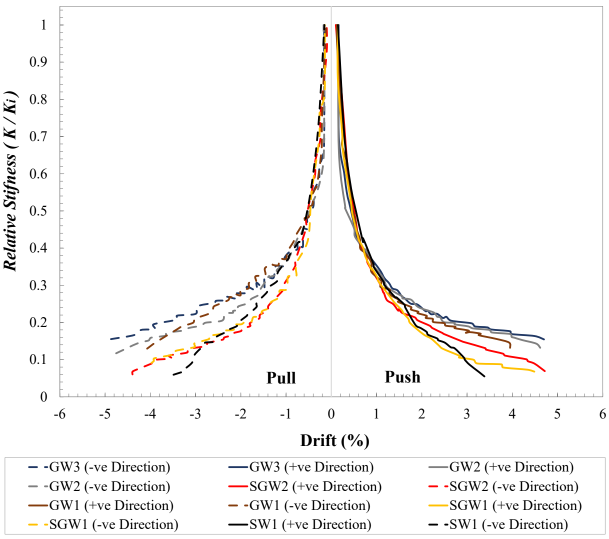

Figure 8 – Normalized stiffness degradation versus drift levels

The currently available approximate equation was used to calculate the fundamental period of vibration as $T_B = 2\pi\sqrt{m/K_s}$, where m is the reactive mass of an equivalent single-degree of- freedom (SDOF) system and K_s is the secant stiffness corresponding with that drift. Considering constant mass, the structural period becomes proportional to $\sqrt{1/K_s}$, and, accordingly, the period shift can be obtained as $T_i = \sqrt{K_i/K_s}\,T_0$, where T_0 is the initial period [18]. The calculated period shifts for each wall are presented in Table 2. At lower damage levels before yielding of steel bars, slightly higher values of calculated period shifts (T/T_0) were attained for GFRP-reinforced walls (1.19, 1.22, 1.28 for walls GW1, GW2, and GW3, respectively) than those of steel-reinforced walls and walls reinforced with a combination of steel and GFRP bars (1.18, 1.19, 1.12 for walls SW1, SGW1, and SGW2, respectively). At the drift level corresponding to concrete spalling, further increases occurred in the calculated period shifts for walls SW1, SGW1, and SGW2 to reach $2.62T_0$, $3.07T_0$, and $2.54T_0$, respectively. In contrast, lower values were attained for GFRP-reinforced walls of, on average, $2.02T_0$. The period shift kept increasing for steel-reinforced walls at a higher rate than those of GFRP-reinforced walls, which is consistent with the stiffness degradation trends in Figure 8.

Table 2 - Summary of experimental damage progression and corresponding fundamental period shift

Characteristic damage Stage	Wall	$\frac{Q}{Q_u}\%$	$\frac{\Delta}{\Delta_{max}}\%$	$\frac{T}{T_0}$
First crack	SW1	35.70	5.22	1.18
	SGW1	28.24	4.51	1.19
	GW1	27.95	5.37	1.19
	SGW2	44.96	4.96	1.12
	GW2	23.59	4.76	1.22
	GW3	23.11	4.70	1.28
Concrete spalling	SW1	90.79	72.20	2.62
	SGW1	70.89	63.33	3.07
	GW1	95.18	65.38	2.30
	SGW2	90.88	59.78	2.54
	GW2	80.92	58.49	2.26
	GW3	94.16	60.91	2.24
Concrete crushing	SW1	-90.66	98.44	4.26
	SGW1	-103.36	88.60	3.83
	GW1	-105.82	100.00	2.75
	SGW2	122.67	100.00	3.72
	GW2	-123.63	100.00	2.75
	GW3	-126.60	100.00	2.54

3.4. Idealized displacement ductility

The idealized lateral load-drift envelope of each tested wall was determined based on the equivalent energy elastic-plastic method [19], as shown in Figure 9. The idealized displacement ductility values μ_Δ^{id} were determined by dividing the maximum lateral displacement by the idealized yield displacement. Figure 10 depicts the idealized backbone curve for all tested walls. Table 3 provides a summary of the idealized response of all tested walls.

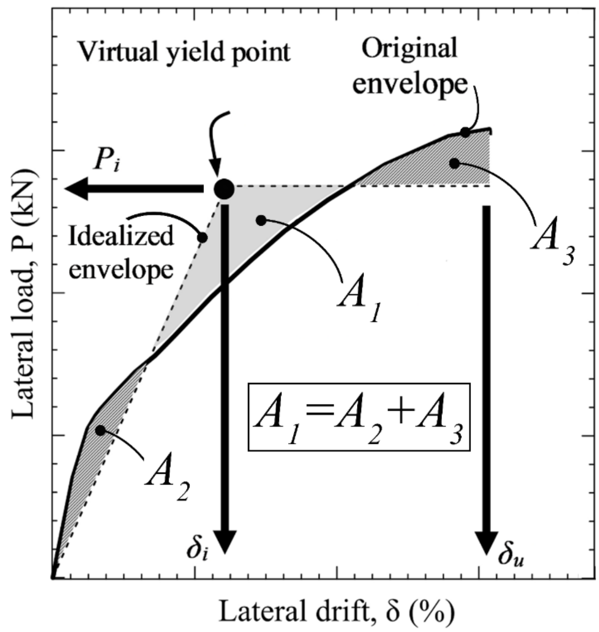

Figure 9 – Bilinear idealization of the lateral load-drift envelope, [18]

According to Figure 10 and , The steel-reinforced wall and hybrid steel-reinforced walls had higher displacement ductility compared to GFRP-reinforced walls. Idealized displacement ductility values (μ_Δ^{id}) of 9.98, 9.22, and 11.84 were attained for walls SW1, SGW1, and SGW2, respectively. The hybrid wall, SGW2, reached a greater peak strength than the control wall (SW1). The increased ductility of wall SGW2, compared to the control wall (SW1), could be attributed to the higher reinforcement ratio of steel rebars at wall edges. However, walls GW1, GW2 and GW3 had lower idealized displacement ductility values than the control steel-reinforced wall. This reduction in displacement ductility is mainly due to the linear elastic behaviour of GFRP bars. While in the case of hybrid steel-reinforced walls, steel bars' high plastic deformation capacity significantly increased the resultant ductility.

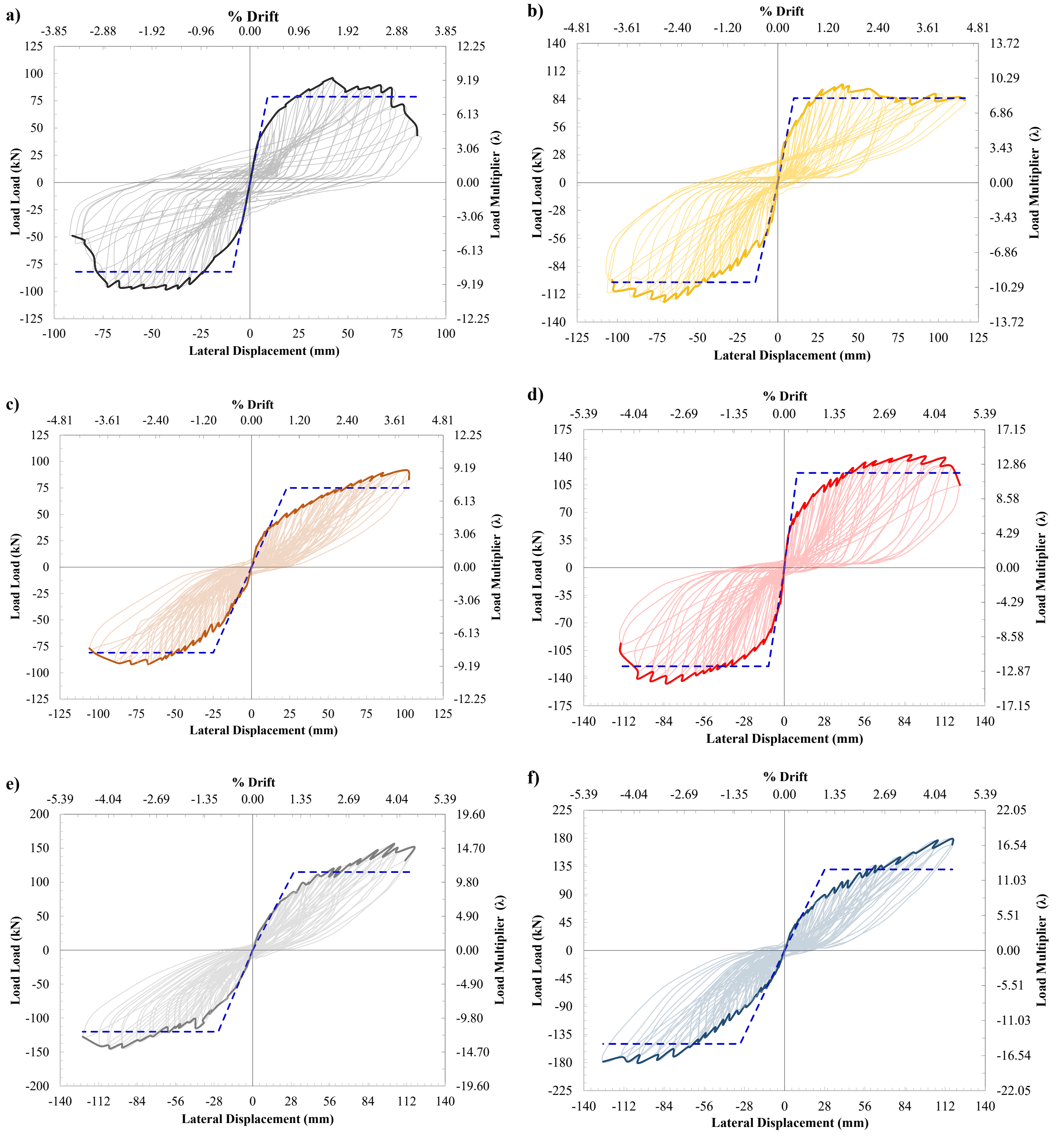

Figure 10 – Hysteretic response, backbone curve, and idealized backbone curve of control wall specimen (a), hybrid steel-GFRP reinforced walls (b&c), and GFRP-reinforced walls (d-e)

Table 3 - Obtained parameters of idealized backbone curves for tested walls

Specimen	**Yield Drift** (%)	**Ultimate Drift** (%)	**Yield Strength** kN	μ_{Δ}^{id}
SW1	0.35	3.45	80.38	9.98
SGW1	0.46	4.26	92.50	9.22
SGW2	0.38	4.56	122.50	11.84
GW1	0.92	4.01	78.00	4.34
GW2	1.06	4.52	117.50	4.28
GW3	1.13	4.68	140.00	4.13

4. Conclusion

The present research was carried out on RC concrete shear walls in order to investigate the capability of using hybrid steel-GFRP reinforcement in reinforcing shear walls to resist seismic loads. Different reinforcement ratios were adopted for the hybrid steel-GFRP reinforced walls and for the GFRP-reinforced walls to thoroughly assess the effect of the GFRP reinforcement ratio on the global behaviour and self-centring performance of RC shear walls. The findings are promising concerning applications for hybrid steel-GFRP reinforcement as the walls achieved their ultimate strength with no sign of premature shear, sliding shear, or instability failure. Moreover, the GFRP-RC walls showed stable hysteretic performance with a higher drift capacity than steel-reinforced walls. Furthermore, the elastic behaviour of GFRP bars resulted in lower damage rates with realigned cracks and recoverable deformation at the same drift level for hybrid steel-GFRP and GFRP-reinforced walls compared to the steel-reinforced wall.

Declaration of Conflict of Interests

The authors declare that there is no conflict of interest. They have no known competing financial interests or personal relationships that could have appeared to influence the work reported in this paper.

References

[1.] Z. Tuna, Seismic Performance, Modeling, and Failure Assessment of Reinforced Concrete Shear Wall Buildings, Los Angeles: PhD Thesis, University of California, 2012.

[2.] K. Orakcal, L. M. Massone ve J. W. Wallace, «Shear Strength of Lightly Reinforced Wall Piers and Spandrels,» ACI Structural Journal, cilt 106, no. 4, pp. 455-465, 2009.

[3.] F. Talaei, Numerical Simulation and Economic Design of Concrete Shear Walls Reinforced with GFRP Bars, Alberta, Canada: M.Sc. Thesis, University of Alberta, 2017.

[4.] W. L. Cortés-Puentes ve D. Palermo, «Modeling of RC Shear Walls Retrofitted with Steel Plates or FRP Sheets,» Journal of Structural Engineering, cilt 138, no. 5, pp. 602-612, 2012.

[5.] C. Kassem, A. S. Farghaly ve B. Benmokrane, «Evaluation of Flexural Behavior and Serviceability Performance of Concrete Beams Reinforced with FRP Bars,» Journal of Composites for Construction, cilt 15, no. 5, pp. 682-695, 2011.

[6.] C. E. Bakis, L. C. Bank, V. L. Brown, E. Cosenza, J. F. Davalos, J. J. Lesko, A. Machida, S. H. Rizkalla ve T. C. Triantafillou, «Fiber-Reinforced Polymer Composites for Construction—State-of-the-Art Review,» Journal of Composites for Construction, cilt 6, no. 2, pp. 73-87, 2002.

[7.] E. El-Salakawy, B. Benmokrane, A. El-Ragaby ve D. Nadeau, «Field Investigation on the First Bridge Deck Slab Reinforced with Glass FRP Bars Constructed in Canada,» Journal of Composites for Construction, cilt 9, no. 6, pp. 470-479, 2005.

[8.] M. K. Sharbatdar ve M. Saatcioglu, «Seismic Design of FRP Reinforced Concrete Structures,» Asian Journal of Applied Sciences, cilt 2, no. 3, pp. 211-222, 2009.

[9.] H. Tobbi, A. S. Farghaly ve B. Benmokrane, «Concrete Columns Reinforced Longitudinally and Transversally with Glass Fiber-Reinforced Polymer Bars,» ACI Structural Journal, cilt 109, no. 4, pp. 551-558, 2012.

[10.] N. Mohamed, A. S. Farghaly, B. Benmokrane ve K. W. Neale, «Flexure and Shear Deformation of GFRP-Reinforced Shear Walls,» Journal of Composites for Construction, cilt 18, no. 2, p. 04013044, 2014.

[11.] D. H. Deitz, I. E. Harik ve H. Gesund, «Physical properties of glass fiber reinforced polymer rebars in compression,» Journal of Composites for Construction, cilt 7, no. 4, pp. 363-366, 2003.

[12.] Y. Chen, J. F. Davalos ve I. Ray, «Durability Prediction for GFRP Reinforcing Bars Using Short-Term Data of Accelerated Aging Tests,» Journal of Composites for Construction, cilt 10, no. 4, pp. 279-286, 2006.

[13.] N. Mohamed, A. S. Farghaly, B. Benmokrane ve K. W. Neale, «Experimental Investigation of Concrete Shear Walls Reinforced with Glass Fiber–Reinforced Bars under Lateral Cyclic Loading,» Journal of Composites for Construction, cilt 18, no. 3, pp. A4014001-1-12, 2014.

[14.] A. Arafa, A. S. Farghaly ve B. Benmokrane, «Experimental Behavior of GFRP-Reinforced Concrete Squat Walls Subjected to Simulated Earthquake Load,» Journal of Composites for Construction, cilt 22, no. 2, pp. 04018003-1-14, 2018.

[15.] M. Z. Afifi, H. M. Mohamed, O. Chaallal ve B. Benmokrane, «Confinement Model for Concrete Columns Internally Confined with Carbon FRP Spirals and Hoops,» Journal of Structural Engineering, cilt 141, no. 9, p. 04014219, 2015.

[16.] S. M. Hosseini, M. Yekrangnia ve A. V. Oskouei, «Effect of spiral transverse bars on structural behavior of concrete shear walls reinforced with GFRP bars,» Journal of Building Engineering, cilt 55, p. 104706, 2022.

[17.] M. Hadzima-Nyarko, H. Draganić, H. Draganić ve T. Štefić, «Comparison of fundamental periods of reinforced shear wall dominant building models with empirical expressions,» Tehnički vjesnik, cilt 22, no. 3, pp. 685-694, 2015.

[18.] I. Shabana, A. S. Farghaly ve B. Benmokrane, «Earthquake response of GFRP-reinforced concrete squat walls with aspect ratios of 1.14 and 0.68,» Engineering Structures, cilt 252 , p. 113556, 2022.

[19.] R. Park, «Ductility evaluation from laboratory and analytical testing,» %1 içinde Proceedings of the 9th World Conference on Earthquake Engineering, Tokyo-Kyoto, Japan, 1988.

How to Cite This Article

el-Kady, H., Amer, O., Ali, A., and Haggag, H., Hysteretic performance of hybrid GFRP-steel reinforced concrete shear walls: An experimental Investigation, Cement Based Composites, 4 (2022), 5736.
https://doi.org/10.36937/cebacom.2022.5736